Boothe, T. J., Mitchell, S. F. and Lentz, D. R. 2022. Mineralogy and geochemistry of Eocene plutons associated with iron skarn mineralisation in the Wag Water Belt, Jamaica. *Caribbean Journal of Earth Science*, **54**, 11-28.
 Available online 9th May 2022.

Mineralogy and geochemistry of Eocene plutons associated with iron skarn mineralisation in the Wag Water Belt, Jamaica

TASHANE J. BOOTHE[1,2], SIMON F. MITCHELL[1], DAVID R. LENTZ[3]

[1] *Department of Geography and Geology, University of the West Indies, Mona, Kingston 6, Jamaica*

[2] *Current Address: Department of Geology and Environmental Science, University of Pittsburgh 4107 O'Hara Street, Pittsburgh, PA 15260-3332, USA. Email: tj_boothe@yahoo.com*

[3] *Department of Earth Sciences, University of New Brunswick, Fredericton, NB E3B 5A3, Canada*

ABSTRACT. The Newcastle Porphyry crops out extensively in the Wag Water Belt, occurring primarily as porphyritic lava flows and shallowly-emplaced intrusions. Compositionally, the Newcastle Porphyry ranges from basaltic andesite to rhyolites. However, unlike normal island arc andesites, dacites, and rhyolites (ARDs), the Newcastle Porphyry has anomalously high SiO_2 (52.5 – 72 wt.%) and Al_2O_3 (7.3 -19 wt.%), low MgO (0.2 - 5.79 wt.%), and negative heavy rare earth element (HREEs) anomalies and is therefore geochemically similar to adakites. In the Mavis Bank district, the Newcastle Porphyry is spatially and genetically associated with calcic iron skarn mineralisation and with minor Cu and Co. The trace element geochemistry of the Newcastle Porphyry is consistent with that of plutons associated with iron skarns worldwide. Critical trace elements such as Rb, Zr, Ba, Sr, and V are within the ranges expected for undifferentiated magmas. The major element composition however shows some variations from the average Fe skarn pluton, with higher SiO_2 and Fe_2O_3 content and lower MgO and K_2O content.

Keywords: Iron skarn; Massive magnetite; Jamaican-type adakite; Newcastle Porphyry.

1. INTRODUCTION

Skarns are geochemically altered rocks dominated by calcsilicate minerals, such as garnet and clinopyroxene. In general, the formation of skarns involves the metasomatism or metamorphism of carbonate-rich rocks by fluids derived from a cooling pluton. Although limestone, dolomite, and shales are the main skarn protoliths, skarns can also be formed from the metasomatism of granite, basalts, and sandstone (**Meinert et al., 2005**). Additionally, metasomatising fluids may also originate from sources other than intrusions, such as geothermal environments, and metamorphic or faulted terranes (**Meinert, 1992**; **Meinert et al., 2005**; **Pirajno, 2009**). In the field, skarn minerals are often mappable and display distinct mineral zonation patterns as a result of the movement of hydrothermal fluids outwards from the cooling pluton (**Meinert, 1997, 2005**).

Skarn deposits are critically important sources of metals such as Fe, Cu, W, Mo, Sn, and Au (**Meinert et al., 2005**). Most deposits are considered small to medium sized when compared to other metal deposits such as epithermal, BIF (banded iron formation), and porphyry deposits. Nevertheless, there are few skarn deposits that are relatively large, for example, the Marcona and Turgai deposits in Peru and Kazakhstan respectively contain over 430 Mt of Fe (**Laznicka, 2006**; **Meinert, 1992**). For this reason, skarns are generally classified by their main ore metals associations, with each skarn type displaying characteristics distinguishable from the others. For example, Fe skarns are typically characterised by average Fe grades of 40% with associated Cu, Au, and Co, and an ore mineral assemblage of magnetite, chalcopyrite, and cobaltite.

It has also been shown in several notable works (c.f., **Meinert, 1995**; **Meinert, 1984**; **Pons et al., 2010**; **Ray et al., 1995**) that the trace and major element composition of skarn plutons worldwide vary depending on the main ore metal in an associated skarn deposit. This suggests that there is a close genetic relationship between the skarn types and the geochemistry of associated causative plutons. Iron skarn mineralisation in Jamaica occurs within the Mavis Bank District (**Figure 1**) and is genetically related to subvolcanic porphyritic andesite-dacite sills or dykes associated with the Newcastle Porphyry. Throughout this paper, these sills or dykes are referred to as 'plutons' or 'causative plutons' which are generalised terminologies used in skarn research to denote the intrusive body responsible for mineralisation.

The Newcastle Porphyry has geochemical signatures akin to early Archean trondjhemites, tonalites and granodiorites (TTG) and Cenozoic adakites (**Hastie et al., 2010, 2015**). Adakites are thought to be formed from the partial melting of

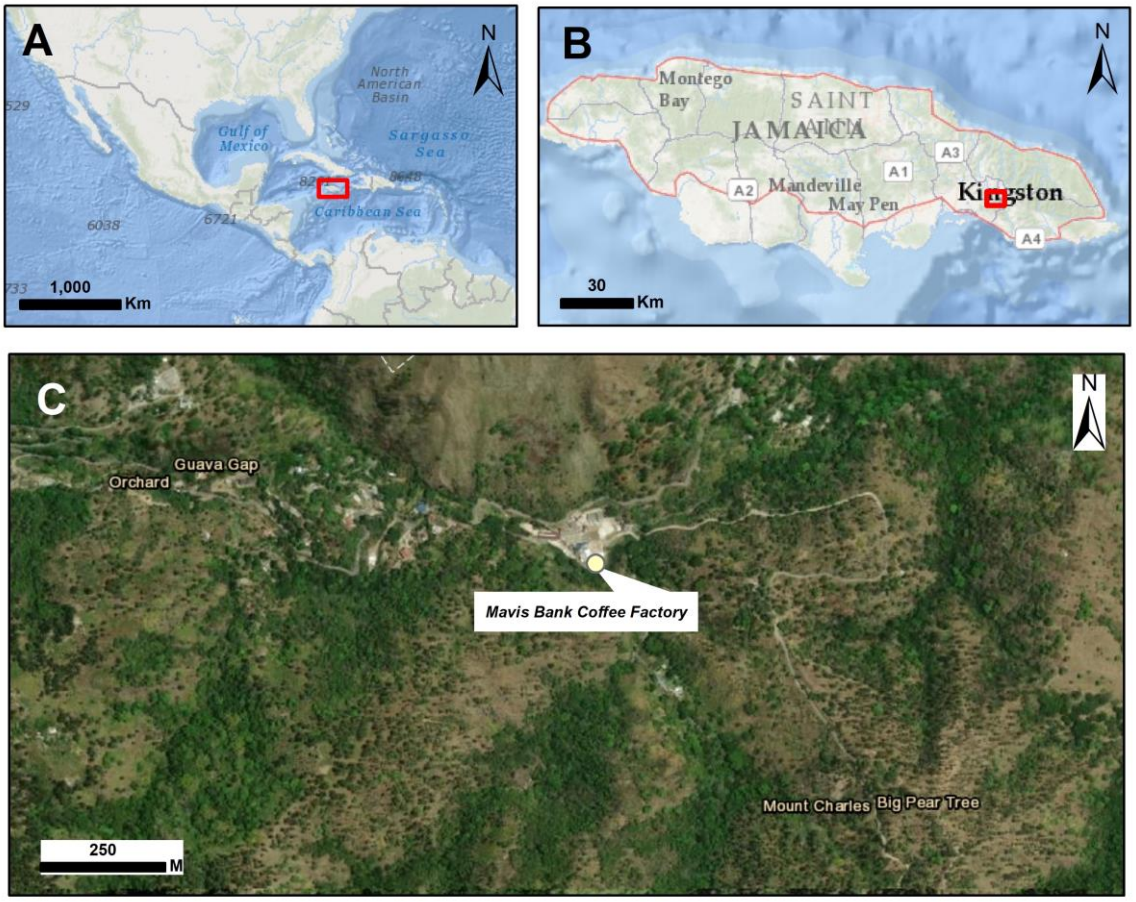

Figure 1. Location of the Mavis Bank area. The area of interest is outlined in blue. A: Jamaica is located 40 km south of Cuba and 190 km west of Hispaniola. B: The area of interest is located in eastern St Andrew parish, near the border with St Thomas parish. Source: Google Earth Image 2019.

subducted oceanic crust that is less than 25 million years old and, as such, display geochemical signatures dissimilar to 'normal' arc-like andesites, dacites, and rhyolites (ADRS). For example, compared to normal ADRs, adakites have high SiO_2 and Na_2O contents, relatively low K_2O, heavy rare earth element (HREE), and Y contents, negative Ta and Nb anomalies on multielement diagrams, and high Sr/Y and La/Yb ratios (**Castillo, 2006, 2012**; **Moyen, 2009**). The Newcastle Porphyry is therefore not only geologically significant in unravelling the tectonic evolution of this region, but also plays a critical role as the source of iron, and minor copper, gold, and cobalt mineralisation in Jamaica.

This study examines the mineralogy, and major and trace element composition of the Newcastle Porphyry within the mineralised areas of the Mavis Bank district. The data is interpreted primarily using several geochemical plots to assess the extent to which the geochemistry of the Newcastle Porphyry is consistent with that of typical Fe skarn related plutons worldwide. We also attempt to account for geochemical anomalies observed in the Newcastle Porphyry and highlight the role of adakitic rocks in skarn mineralisation.

2. GEOLOGY

The geological evolution of the Caribbean Plate, and by extension Jamaica, has been widely researched (e.g., **Kerr et al., 1999**; **Pindell et al., 2006**; **Pindell and Kennan, 2009**; **Hastie and Kerr, 2010**; **Mitchell, 2020**), although there is little consensus on several key aspects of the different models. Despite the ongoing debate, it has been widely accepted that the Caribbean Plate had its origin in the Pacific as the Caribbean Large Igneous Province (CLIP). An eastward migration of the plate relative to the Americas led to a subduction polarity reversal and subsequent subduction of Proto-Caribbean oceanic crust beneath the CLIP. Eventually, in the Paleocene to Early Eocene, the northern margins of the CLIP collided with, and

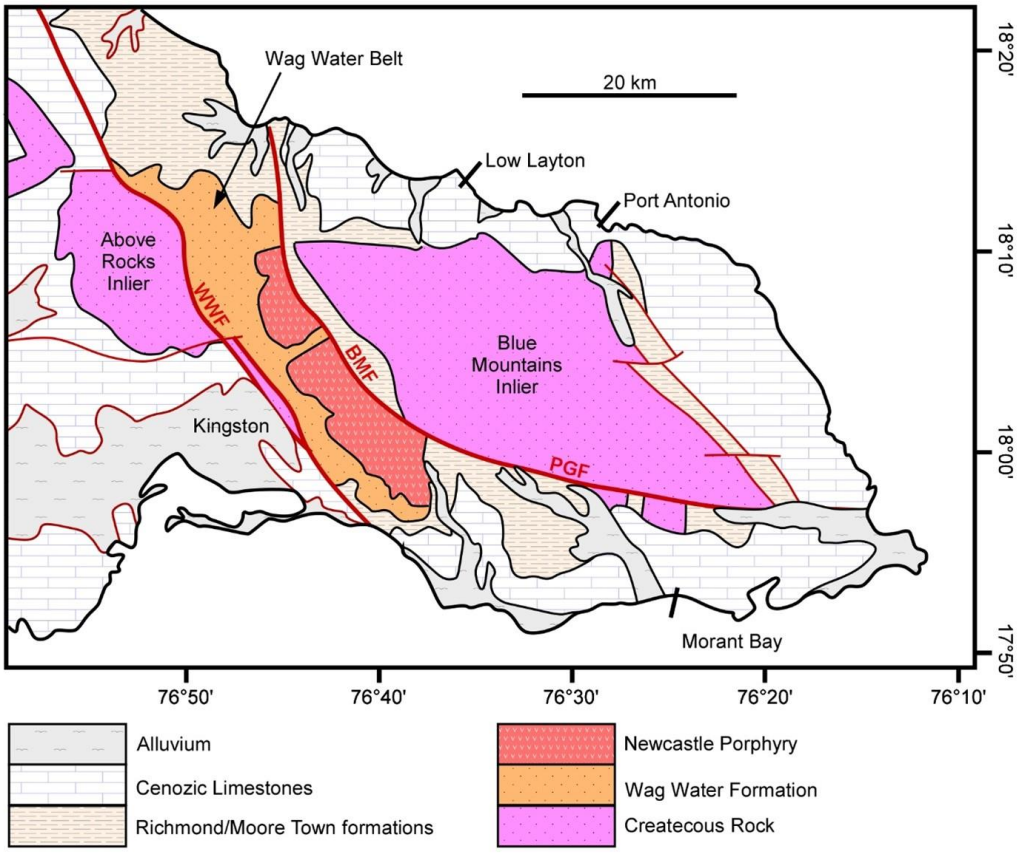

Figure 2. Simplified geology of eastern Jamaica. WWF-Wag Water Fault, BMF-Blue Mountain Fault, PGF-Plantain Garden Faultmeteredited from Mines and Geology Division, 1998).

under thrusted Jamaica (**Pindell, 1994**; **Pindell et al., 2006**; **Hastie and Kerr, 2010**).

2.1 Regional and Local Geology

The oldest exposed rock units in Jamaica are a succession of volcanic and volcanogenic rocks, shallow-water limestones, shallow-water conglomerates, deep-water marine shales and sandstones, and low-grade metamorphic rocks of Early to Late Cretaceous age that are exposed in a series of inliers across the island (**Robinson et al., 1970**; **Roobol, 1971**; **Robinson, 1994**; **Robinson and Mitchell, 1999**; **Mitchell, 2003a, 2006, 2020**). The 7 km-wide, 50 km-long Wag Water Belt (**Figure 2**) is a tectonic feature in eastern Jamaica that formed in the Palaeocene to early Eocene through rifting of Cretaceous rocks but has been subsequently inverted during the last 12-14 Mys (**James-Williamson et al., 2014**). The belt contains a 7 to 9 km thick sequence of clastic sedimentary rocks intercalated with igneous rocks that are overlain by mid-Paleogene to early Neogene carbonates (**Mann and Burke, 1990**; **Robinson, 1994**; **Robinson and Mitchell, 1999**; **Mitchell, 2003b**). The clastic sedimentary rocks consist of a thick lower unit of predominantly terrestrial conglomerates (Wag Water Formation) and a thick upper unit of deep-water, interbedded shales and sandstones (Richmond Formation). The Wag Water Formation contains numerous thin marine intercalations, represented by sandstones and conglomerates, shales, up to 100 m thick limestone units, and at least one interval with evaporites (gypsum and anhydrite). However, recent geological mapping indicates that this simple succession as proposed by **Mann and Burke (1990)** can be mapped as lithologically distinct rock units (**Mitchell, 2021**).

The clastic sedimentary rocks of the Wag Water Belt are intercalated with igneous rocks. In the literature, these have been referred to as the Newcastle Volcanics (calc-alkaline dacites or quartz keratophyres: **Jackson and Smith, 1978**; **Jackson, 1987**; **Roobol, 1975**) and the Halberstadt Volcanics (basalts) (**Matley, 1940**; **Hastie et al., 2011**). Yet the term 'volcanics' implies an extrusive origin for these rocks and various stratigraphic guides (e.g.,

Murphy and Salvador, 1998, p. 260) indicate that this term should not be used for rock units. **Hastie et al.** (**2010**) obtained early Eocene Ar-Ar dates (52.74 ± 0.34 Ma) on dacites from the southern Wag Water Belt that are associated with Palaeocene limestones, which suggests that the dated rocks are intrusions (probably sills) to which the term 'volcanics' is not appropriate. We therefore prefer to revert to the terms 'Newcastle Porphyry' (**Matley, 1940**) and Halberstadt Basalt to refer to these suites of intrusive and extrusive igneous rocks.

Hastie et al. (**2010**) determined that the Newcastle Porphyry (which plotted as a rhyodacite on discriminant diagrams) was characterised by high silica (64.6-72.2 wt.%), high Al_2O_3 (14.5-16.0 wt.%), high Na_2O (3.8-7.6 wt.%), low MgO (≤ 2 wt.%) and low K_2O (0.1-1.1 wt.%), which suggests that they can be classified as adakites. Trace-element concentrations are also similar to adakites; they have relatively low La/Yb ratios, low Y and Yb concentrations, negative Ti and P anomalies, concave middle to heavy REEs, Gd/Yb ratios greater than 1, and negative Nb and Ta anomalies on a primitive mantle-normalised diagram (**Defant and Drummond, 1990**; **Martin, 1999**; **Castillo, 2006**; **Hastie et al., 2010, 2015**). The main distinction between the Newcastle Porphyry and modern adakites is a relatively low Sr concentration coupled with low Sr/Y ratios. To explain the distinctive geochemistry (high SiO_2 and Al_2O_3, low MgO, and negative HREE anomalies), **Hastie et al.** (**2010, 2015**) proposed that the rocks of the Newcastle Porphyry were derived from 15-30% partial melting of a garnet amphibolite source that represents the metamorphosed CLIP that underthrust Jamaica. Furthermore, the geochemistry of the Newcastle adakites suggested only limited interaction and hybridization with a thin mantle wedge above the subducted CLIP or that mantle signatures were erased during fractional crystallisation (**Hastie et al., 2010, 2015**). One mechanism to explain their generation is through decompression melting of the subducted CLIP during the crustal extension that produced the Wag Water Rift (**Hastie et al., 2010**).

2.2 Skarn Mineralisation

In a 1960 economic minerals survey, International Metals Ltd identified massive lenticular iron as the main ore type in the Mavis Bank area. These vein-like structures are associated with pyrite, calcite, and silicates that partially or completely replace limestone. The iron content in these ores ranges from 30-67 wt.%. The tabular or lenticular bodies have an average thickness of 6 m with vertical to near-vertical dips, and extend up to 46 m below the surface (**Vincenz, 1955**; **Zans, 1955**). Faulting within the region has dissected these magnetite bodies producing discontinuous strikes and, in some cases, detached massive iron boulders (**Blaise and Fenton, 1976**).

Magnetic and Audio Frequency Magnetics (AFMAG) surveys within the mineralised zones revealed "solid and high grade" intergrowths of magnetite and hematite with iron content of up to 65 wt.% (**Vincenz, 1955**). Hematite was identified as the dominant mineral in most areas that showed little or no magnetism (**Vincenz, 1955**). Other mineralisation types identified include iron-copper bodies with disseminated chalcopyrite and pyrite, Cu-Fe skarns in shales and limestones (with chalcopyrite and specularite), low-grade copper in porphyry, and copper replacement of limestone (**Blaise and Fenton, 1976**).

3. METHODOLOGY

The Newcastle Porphyry is the subject of investigation in this study. We utilised whole rock major and trace element analysis as the main geochemical techniques supplemented by petrographic and thin section analyses. The techniques are described below.

3.1 Field Excursion

Field assessments were conducted over several visits to the study area, starting in August 2014. This assessment involved sampling of the main lithologies, with special attention being paid to outcrops of the Newcastle Porphyry and the mineralised zones. In most areas, the outcrops were highly weathered, and so sampling of fresh, unaltered igneous rocks was difficult. Systematic sampling of the study area within grids was not possible due to the rugged terrain and the lack of access roads.

In lieu of detailed geological mapping, the 1:4,000 geology map produced by **Blaise and Fenton** (**1976**) was used as a base map. Verifications and amendments were made, as needed, in areas that were accessible. Mapping also recorded faults and strike and dip data where available. Scaled photographs of the outcrops were also taken.

3.2 Petrographic Analysis

Polished thin sections of various lithologies (thickness of 30 microns) were made at the University of New Brunswick, Canada. The

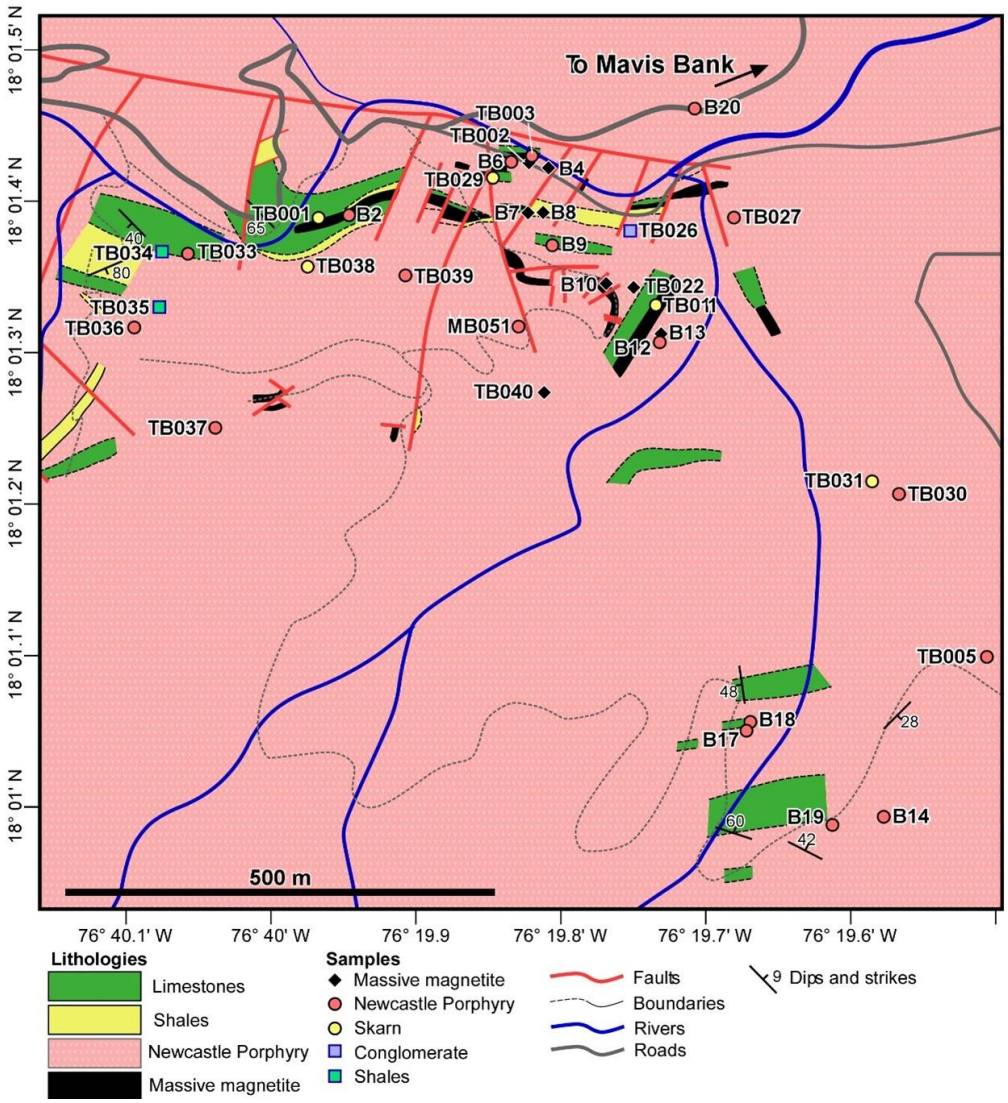

Figure 3. Geology of the Mavis Bank area showing massive magnetite exposure on surface. Modified after Blaise and Fenton (1976).

polished thin sections were examined at the Mines and Geology Division, Jamaica, using a Censico Trinocular petrographic microscope outfitted with a 35 mm SLR camera. Samples were interpreted using plane and cross polarised transmitted and reflected light. Photomicrographs were taken at the Microscopy Unit at the University of the West Indies, Jamaica, with a Leica DMRME Optical Microscope outfitted with a Lumenera Infinity 1 Digital Camera.

3.3 Major Element Analysis

Major element analysis was conducted at the Mines and Geology Division Laboratory in Kingston, Jamaica, using a Perkin Elmer A3100 flame atomic absorption spectrometer (FAAS). These data are essential for the classification of the Newcastle rocks as adakites and are also useful in differentiating igneous rock types and geological settings. However, the use of major elements on the total alkali-silica (TAS) diagram as a means of classifying altered or weathered igneous rocks, as is the case of the Newcastle Porphyry, is not encouraged. This is due to the high mobility of the elements used in the classification which reduces the reliability of the plots obtained (**Jenner, 1996**; **Hastie et al., 2007**). The use of immobile trace elements as proxies for major elements is demonstrably more valuable. Nevertheless, major element data were normalised to 100% with LOI and then recalculated to anhydrous values without LOI.

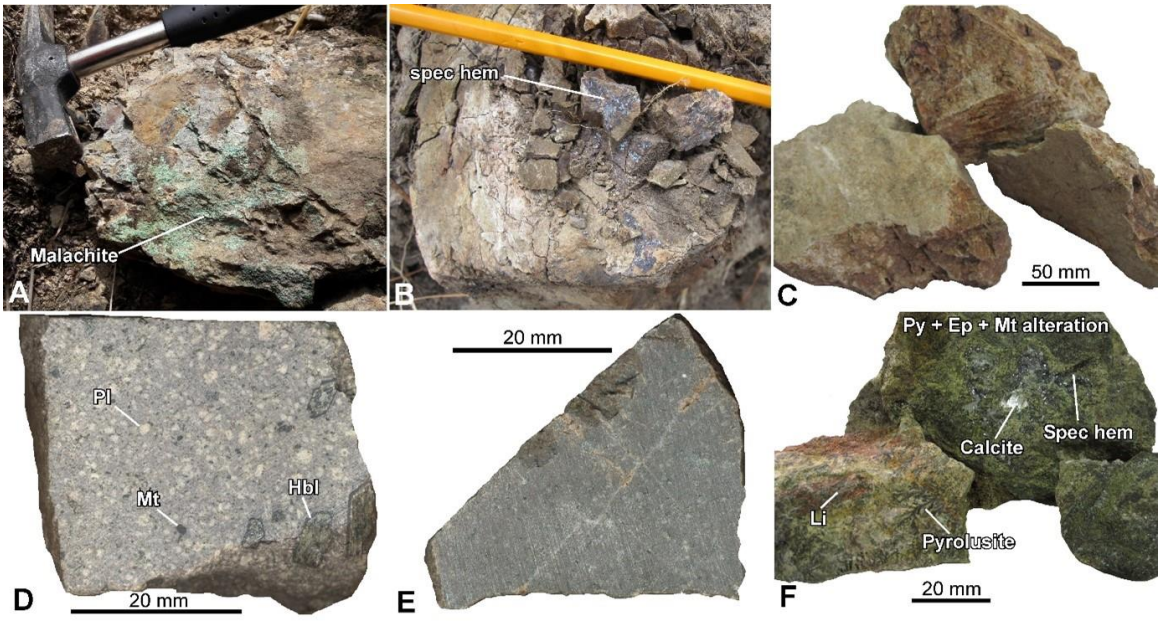

Figure 4. Newcastle Porphyry outcrop and hand specimens. A: Supergene malachite mineralisation. B: Specularite mineralisation. C: Highly weathered, unmineralised specimen. D: Un-mineralised porphyry with large phenocrysts of plagioclase (Pl), magnetite (Mt), and altered hornblende (Hbl). E: Microgranitic texture with acicular hornblende crystals and plagioclase phenocryst. F: Porphyry showing pervasive propylitic alteration. Epidote (Ep) and magnetite (Mt) overprints the original mineralogy. Iron also occurs as specular hematite and pyrite (Py) with secondary limonite. Pyrolusite and calcite are locally present.

3.4 Trace Element Analysis

Trace element analyses were conducted at the ActLabs in Ontario, Canada using instrumental neutron activation analysis (INAA) (see **Hoffman, 1992**). To obtain a wider range of trace elements with lower detection limits, samples were also analysed using inductively coupled mass spectrometry (ICP-MS) at the Bureau Veritas Lab in Vancouver, Canada (**Hall, 1992**).

The use of immobile trace elements is considered a more reliable method of classifying volcanic rocks, volcanic rock series, and tectonic setting (**Jenner 1996**; **Hastie et al. 2007**; **Pearce 2014**). In this study, the Nb/Y-Zr/Ti and Th-Co diagrams are used as proxies for the TAS and the K_2O-SiO_2 diagrams respectively.

4. Results

The Newcastle Porphyry intrudes sections of the Wag Water Formation and has resulted in the metasomatism and low-grade metamorphism of the limestone facies (Good Hope Limestone) primarily in the areas south of the Mavis Bank Coffee Factory. The geology of the main mineralised zones is updated from a map produced by **Blaise and Fenton (1976)** and shown in **Figure 3**.

4.1 Pluton Geology and Mineralogy

Fresh samples of the Newcastle Porphyry are difficult to locate. The texture and fabric of the rock are often difficult to ascertain since mineralisation, intense alteration and tropical weathering overprints the original rock fabric. In some areas, alteration assemblages have completely replaced the primary mineral assemblages. Mineralisation is most prominent at, or near the contact with massive magnetite lenses. Magnetite, specular hematite, and minor malachite are the main metallic minerals observed in these altered rocks (**Figures 4A-C**)

The Newcastle Porphyry, where unaltered and weakly mineralised, tends to have relatively large anhedral to euhedral phenocrysts of plagioclase, hornblende, and quartz, set in a grey microcrystalline groundmass (**Figure 4D-E**). In thin section (**Figure 5**), some plagioclase crystals appear to be altered to sericite and may also have fracture-controlled intergrowths of chlorite. Hornblende is generally highly altered and, in most cases, has been altered to chlorite and sericite. In some areas, the intrusions are mineralised with iron occurring as disseminated magnetite and as veins less than 1 mm in width. In thin section, magnetite has a close relationship with epidote and frequently occurs as an intergrowth within fine aggregates or elongated crystals of epidote. Iron also occurs as hematite and

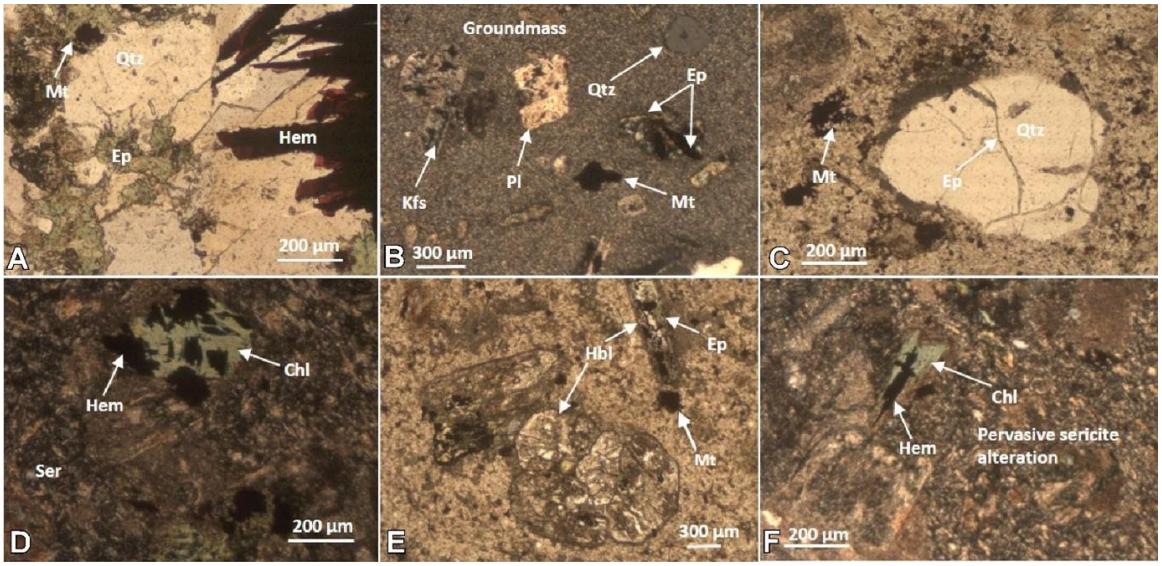

Fig. 5. Photomicrographs of the Newcastle Porphyry in thin section (transmitted light (plane polarised) petrography). A: Alteration assemblage of quartz (Qtz), epidote (Ep), hematite (Hem), and magnetite (Mt). B: Potassium feldspar (Kfs), plagioclase (Pl), quartz (Qtz), and epidote (Ep) phenocrysts in an aphanitic groundmass. C: Quartz phenocryst showing epidote growth in fractures. Clay minerals also occur on the rim of the crystal. Magnetite (Mt) occurs as disseminations. D: Altered porphyry with hematite (Hem) overgrowth on chlorite (Chl). E: Hornblende (Hbl) phenocryst in cross section and longitudinal section. Hbl is highly altered to magnetite and epidote. F: Hematite (Hem) occurs as replacement in chlorite (Chl). Sericitic alteration is pervasive in the groundmass.

Figure 6. Massive magnetite in outcrop and hand specimen. A. Fresh surface of magnetite-rich, dense skarn. B: Pyroxene-rich skarn. C: Low grade marble with Fe-Mn rich veins typical of distal skarn. D: Fragmented massive magnetite with calcite vein partially covered by overburden. E: Partially martitized massive magnetite with voids. F: Massive magnetite in contact with altered porphyry. The contact between the magnetite and volcanic rock is sharp. Large euhedral pyrite is common.

specular hematite with secondary limonite (**Figure 6**). Dendritic pyrolusite and the secondary copper mineral malachite are also common in these rocks. Calcite is rarely observed in hand specimen, but can occur as 1 cm wide clusters of euhedral crystals. The alteration assemblage of epidote, calcite,

potassium feldspar, and plagioclase indicates that the rocks have undergone propylitic alteration.

4.2 Major element Geochemistry

Silica content is variable in the Newcastle Porphyry, ranging from 52.5 to 72.3 wt.%. The total alkali ($Na_2O + K_2O$) is also variable and ranges from 1.2 to 8.5 wt.%. MgO ranges from a high of 5.97 wt.% to a low of 0.20 wt.%, whereas Al_2O_3 ranges from 7.3 to 19.0 wt.%.

Fe_2O_3 content averages 5.95 wt.%, with a high of 21.19 wt.% in one sample. This generally high Fe content is a result of magnetite and hematite (exoskarn) mineralisation. High CaO content of 9.22 to 10.96 wt.% can be attributed to propylitic alteration that was observed in several areas. The detailed major element results are shown in **Table 1**.

4.3 Trace element Geochemistry

The results of trace element analysis are detailed in **Table 2** and **3**. A bivariate plot of Nb/Y vs Zr/Ti which is a proxy for the total alkali-silica (TAS) plot, shows that the majority of the samples are basaltic andesite or andesitic (**Figure 7**). Similarly, on the Th-Co diagram (**Figure 8**) which was developed as a substitute for the K_2O-SiO_2 diagram, the Newcastle Porphyry falls in the basaltic andesite/andesite field, and dacite-rhyolite field. As it relates to the magma series, the Newcastle Porphyry has a calc-alkaline affinity.

A review of the data also revealed that trace elements critical in the definition of adakites are generally within expected ranges. The concentration of Y ranges between 6.8 and 16.5 ppm and Yb ranges from < 0.2 to 1.82 ppm, which are generally higher and lower respectively than data obtained by **Hastie et al. (2010)**. Chondrite-normalised La ranges between 30.3 and 116 ppm with only one sample falling outside the typical range of 40 to 150 ppm for adakites. In addition, chondrite-normalised $(La/Yb)_{cn}$ ranges from 6 to 152, with three samples falling below the typical minimum value of 10. Except for one sample analysed, the Newcastle Porphyry has Sr < 400 ppm, which is a departure from what is typical of adakites. For all samples, the concentration of Ni and Cr ranges from 10.5 to 37.2 ppm and 8 to 97 ppm, respectively. The Ni, Cr, and Sr data are in similar ranges as those obtained by **Hastie et al. (2010)**.

The Sr/Y vs Y and $(La/Yb)_{cn}$ vs Yb_{cn} discriminant diagrams (after **Martin, 1999**) are useful in distinguishing adakites from normal island arc lavas. On the Sr/Y vs Y discrimination diagram (**Figure 9**), the Newcastle Porphyry mostly plots in the adakite field. Nevertheless, the results highlight the low Sr/Y ratios of the Newcastle Porphyry with some samples plotting below the adakite field. This can be attributed to the very low Sr values ranging from 59.3 to 463 ppm which are below the typical value for adakites (>400 ppm). On the other hand, the values of Y for all samples are below 18 ppm, which is typical of adakites.

The $(La/Yb)_{cn}$ vs Yb_{cn} discrimination diagram (**Figure 10**) shows that twelve of the fifteen samples plot within the adakite field. As in the previous diagram, the concentration of the rare earth elements is low, and this results in low $(La/Yb)_{cn}$ ratios. As such, most of the samples plot as a cluster within the lower section of the adakite field.

A plot of the primitive-mantle normalised values for 25 trace elements (**Figure 11**) shows that, for the most part, the Newcastle Porphyry has similar compositions to adakites including a relatively depleted HREE (Eu-Lu) pattern and a negative Nb-Ta anomaly. The field outlined represents early Archean tonalites-trondhjemites-granodiorites/dacites (TTG/D) and Cenozoic adakite data compiled by **Hastie et al. (2010)** from various authors. However, unlike late Archean TTG/D and Cenozoic adakites, the Newcastle Porphyry tends to have lower K contents. Overall, when compared to early Archean TTG/D and Cenozoic adakites, the trace element concentration of the Newcastle Porphyry tends to be on the lower ranges of the spectrum.

5. DISCUSSION

5.1 Genesis of the Newcastle Porphyry

The textures of the Newcastle Porphyry show variations in the size and composition of phenocrysts as well as the degree of alteration and mineralisation. This suggests that intrusions were emplaced at varying depths and times during magma evolution. The intrusions associated with the skarns tend to have mirco-phenocrysts and are extensively altered and mineralised, suggesting shallower emplacement than intrusions elsewhere in the study area.

The presence of the calc-alkaline Newcastle Porphyry in the Wag Water rift basin might be considered anomalous where volcanism might be expected to be characterized by tholeiitic lavas resulting from decompression partial melting of the mantle. Major and trace element analysis including multi-element diagrams and bivariate plots of Sr/Y vs Y and $(La/Yb)_{cn}$ vs Yb_{cn} using data generated by this study confirm that the Newcastle Porphyry has

Table 1. Major element concentration of samples of the Newcastle Porphyry within the Mavis Bank area

Parameter	B2	B6	B12	B14	B17	B18	B19	B20	MB51	TB037	TB033	TB039	TB036	TB030	TB005	TB027	TB003
SiO_2 wt.%	66.72	59.47	67.98	57.12	62.34	68.97	59.29	66.95	70.08	70.25	70.20	62.68	52.45	72.26	56.41	70.35	69.52
TiO_2 wt.%	0.05	0.08	0.02	0.05	0.04	0.04	0.03	0.02	-	0.82	0.77	0.97	0.61	-	1.19	0.75	0.81
Al_2O_3 wt.%	17.67	17.58	16.35	17.94	18.08	19.00	21.80	16.79	17.04	15.41	15.10	17.23	7.27	16.71	17.18	14.83	14.14
Fe_2O_3 wt.%	5.27	8.05	4.71	7.16	5.07	2.63	12.00	6.10	1.94	2.92	2.94	3.51	21.19	3.62	7.90	2.66	3.48
MnO wt.%	0.11	0.13	0.11	0.15	0.06	0.08	0.15	0.09	0.09	0.06	0.06	0.05	0.31	0.02	0.15	0.04	0.11
MgO wt.%	1.25	0.34	1.67	3.22	0.26	1.12	0.57	1.40	0.86	0.88	1.11	1.23	5.97	1.20	4.77	0.87	1.49
CaO wt.%	4.60	9.72	5.30	9.51	9.22	3.07	1.59	3.70	6.10	4.41	2.60	5.35	10.96	0.45	3.86	2.75	3.25
Na_2O wt.%	3.63	3.93	3.69	2.89	3.21	3.31	3.08	3.26	3.27	4.85	5.65	8.27	1.10	5.58	8.35	7.31	6.79
K_2O wt.%	0.70	0.71	0.17	1.96	1.73	1.78	1.49	1.69	0.63	0.40	1.58	0.71	0.13	0.16	0.19	0.44	0.43

Table 2. Trace element concentration of samples of the Newcastle Porphyry within the Mavis Bank area (ICP-MS)

Method	Element	Detection Limit	MB51	B2	B6	B12	B14	B17	B18	B19	B20
LF100	Ba ppm	1.0	2617.0	92.0	73.0	71.0	397.0	967.0	126.0	361.0	346.0
LF100	Be	1.0	<1	<1	<1	1.0	<1	<1	<1	<1	<1
LF100	Co	0.2	2.6	8.4	20.5	8.7	14.9	4.4	6.1	31.0	10.8
LF100	Cs	0.1	<0.1	0.2	0.2	<0.1	0.7	0.5	0.6	0.2	0.2
LF100	Ga	0.5	14.4	13.8	15.5	14.1	14.0	16.0	15.5	21.1	16.6
LF100	Hf	0.1	2.8	3.1	2.8	3.3	3.4	3.7	3.2	3.0	3.9
LF100	Nb	0.1	3.9	7.1	3.9	13.3	5.6	5.0	3.5	5.6	8.6
LF100	Rb	0.1	8.9	15.2	12.3	2.3	38.9	34.2	34.2	28.5	20.5
LF100	Sn	1.0	<1	<1	1.0	<1	<1	<1	<1	1.0	2.0
LF100	Sr	0.5	305.8	160.8	155	105.6	270.7	219.6	59.3	220.4	463.0
LF100	Ta	0.1	0.2	0.6	0.3	1.0	0.3	0.4	0.2	0.3	0.8
LF100	Th	0.2	1.9	3.1	2.2	3.9	3.1	2.2	2.0	3.7	3.4
LF100	U	0.1	0.5	1.0	1.6	1.5	1.3	0.7	0.7	1.5	1.3
LF100	V	8.0	45.0	46.0	75.0	38.0	136.0	77.0	61.0	166.0	48.0
LF100	W	0.5	1.1	<0.5	<0.5	<0.5	0.9	<0.5	<0.5	1.1	<0.5
LF100	Zr	0.1	113.5	126.7	106.7	147.3	129.1	140.1	129.0	106.5	169.7
LF100	Y	0.1	6.8	7.7	8.1	8.7	16.5	7.3	8.4	12.6	9.6
LF100	La	0.1	15.8	12.4	13.4	7.2	16.5	13.5	15.1	21.5	20.8
LF100	Ce	0.1	22.5	19.4	21.2	14.1	29.7	19.0	19.1	32.4	32.8
LF100	Pr	0.02	2.31	2.12	2.25	1.61	3.67	2.16	2.19	3.66	3.51
LF100	Nd	0.3	8.5	7.7	8.2	6.2	15.9	8.10	8.2	13.7	12.4
LF100	Sm	0.05	1.77	1.56	1.67	1.22	3.19	1.56	1.37	2.39	2.33
LF100	Eu	0.02	0.70	0.57	0.66	0.35	0.90	0.65	0.57	0.80	0.79
LF100	Gd	0.05	1.67	1.53	1.55	1.29	3.05	1.58	1.58	2.31	2.27
LF100	Tb	0.01	0.23	0.24	0.26	0.23	0.48	0.23	0.24	0.34	0.34
LF100	Dy	0.05	1.33	1.38	1.48	1.41	2.84	1.28	1.29	2.16	1.84
LF100	Ho	0.02	0.24	0.28	0.27	0.28	0.58	0.24	0.26	0.47	0.38
LF100	Er	0.03	0.62	0.76	0.8	0.88	1.64	0.63	0.75	1.59	1.05
LF100	Tm	0.01	0.07	0.11	0.10	0.12	0.24	0.09	0.10	0.25	0.14
LF100	Yb	0.05	0.51	0.72	0.66	0.81	1.56	0.63	0.56	1.82	0.90
LF100	Lu	0.01	0.09	0.11	0.09	0.13	0.26	0.09	0.09	0.30	0.14
MA200	Mo	0.1	3.9	1.6	7.6	1.9	1.6	1.9	1.2	0.9	4.4
MA200	Cu	0.1	25.0	16.3	252.9	10.4	9.2	18.9	3.1	7.9	41.2
MA200	Pb	0.1	7.1	2.6	1.8	1.2	2.8	0.4	0.1	1.5	3.7
MA200	Zn	1.0	16.0	30.0	7.0	25.0	33.0	3.0	6.0	77.0	69.0
MA200	Ag	0.1	<0.1	<0.1	<0.1	<0.1	<0.1	<0.1	<0.1	<0.1	0.1

Table 2 (continued)

Method	Element	Detection Limit	MB51	B2	B6	B12	B14	B17	B18	B19	B20
MA200	Ni	0.1	10.5	27.7	16.0	22.5	15.2	16.3	12.9	37.2	15.1
MA200	Co	0.2	2.6	8.3	20.5	8.7	15.3	5.1	6.8	28.6	10.9
MA200	Mn	1.0	603.0	684.0	816.0	658.0	920.0	358.0	501.0	983.0	561.0
MA200	Fe (%)	0.01	1.04	3.09	4.58	2.97	4.27	3.26	1.69	7.13	3.82
MA200	As	1.0	<1	5.0	3.0	5.0	4.0	3.0	3.0	6.0	4.0
MA200	U	0.1	0.2	0.4	0.5	0.6	0.6	0.2	0.2	0.7	0.9
MA200	Th	0.1	1.6	2.0	0.9	1.8	2.1	0.6	0.9	1.5	2.4
MA200	Sr	1.0	301.0	161.0	135.0	100.0	252.0	217.0	60.0	197.0	409.0
MA200	Cd	0.1	<0.1	0.1	0.1	0.1	<0.1	<0.1	<0.1	<0.1	<0.1
MA200	Sb	0.1	0.2	0.2	0.6	0.2	0.7	0.3	0.2	0.3	0.2
MA200	Bi	0.1	<0.1	<0.1	<0.1	<0.1	<0.1	0.1	<0.1	<0.1	<0.1
MA200	V	1.0	36.0	44.0	74.0	37.0	136.0	81.0	51.0	153.0	50.0
MA200	Ca (%)	0.01	3.79	2.57	5.19	2.86	4.93	3.38	1.65	0.73	1.77
MA200	P (%)	0.001	0.038	0.054	0.034	0.062	0.065	0.046	0.041	0.074	0.063
MA200	La	0.1	10.4	6.7	7.5	4.8	12.6	7.1	9.8	8.3	13.5
MA200	Cr	1.0	81.0	53.0	68.0	46.0	61.0	74.0	46.0	47.0	97.0
MA200	Mg (%)	0.01	0.42	0.65	0.16	0.93	1.38	0.09	0.68	2.38	0.73
MA200	Ba	1.0	2828.0	91.0	73.0	69.0	381.0	964.0	133.0	336.0	331.0
MA200	Ti (%)	0.001	0.141	0.163	0.135	0.169	0.377	0.206	0.153	0.374	0.258
MA200	Al (%)	0.01	6.53	6.45	5.96	6.51	6.97	7.2	8.47	8.04	6.77
MA200	Na (%)	0.001	4.277	4.453	5.053	5.011	2.633	4.051	4.128	3.792	3.965
MA200	K (%)	0.01	0.38	0.54	0.41	0.09	1.39	1.3	1.37	1.03	1.19
MA200	W	0.1	0.4	0.1	0.5	0.6	0.6	0.2	0.2	0.7	0.2
MA200	Zr	0.1	8.6	22.9	26.2	65.9	27.2	20.7	19.8	12.3	142.4
MA200	Ce	1.0	15.0	13.0	12.0	11.0	23.0	12.0	14.0	15.0	23.0
MA200	Sn	0.1	0.7	0.5	1.0	0.7	0.9	0.7	1.0	1.0	1.6
MA200	Y	0.1	4.9	5.5	4.4	4.6	12.7	3.1	5.3	5.8	8.0
MA200	Nb	0.1	2.7	6.5	2.7	11.8	4.5	4.4	2.5	5.3	8.2
MA200	Ta	0.1	0.2	0.5	0.2	0.9	0.3	0.3	0.2	0.3	0.6
MA200	Be	1.0	<1	<1	<1	<1	<1	<1	<1	<1	<1
MA200	Sc	10.	5.0	5.0	5.0	4.0	14.0	6.0	6.0	20.0	6.0
MA200	Li	0.1	6.6	17.3	5.2	14.5	12.2	2.1	8.9	40.2	14.9
MA200	S (%)	0.1	<0.1	<0.1	<0.1	<0.1	<0.1	<0.1	<0.1	<0.1	<0.1
MA200	Rb	0.1	5.6	9.2	4.7	1.1	29.2	26.9	27.5	12.3	15.1
MA200	Hf	0.1	0.4	0.6	0.8	1.5	0.9	0.5	0.6	0.4	3.2
MA200	In	0.05	<0.05	<0.05	0.06	0.05	0.05	<0.05	<0.05	<0.05	<0.05
MA200	Re	0.005	<0.005	<0.005	<0.005	<0.005	<0.005	<0.005	<0.005	<0.005	<0.005
MA200	Se	1.0	<1	<1	1.0	<1	<1	<1	<1	<1	<1
MA200	Te	0.5	<0.5	<0.5	<0.5	<0.5	0.7	<0.5	<0.5	<0.5	<0.5
MA200	Tl	0.5	<0.5	<0.5	<0.5	<0.5	<0.5	<0.5	<0.5	<0.5	<0.5

Table 3. Trace element concentration of samples of the Newcastle Porphyry within the Mavis Bank area (INAA)

Analyte Symbol	Detection Limit	TB003	TB005	TB027	TB030	TB033	TB036	TB037	TB039
Au (ppb)	2.0	< 2	< 2	< 2	< 2	< 2	< 2	< 2	< 2
Ag ppm	5.0	< 5	< 5	< 5	< 5	< 5	< 5	< 5	< 5
As	0.5	< 0.5	< 0.5	< 0.5	2.4.0	< 0.5	19.8	< 0.5	< 0.5
Ba	50.0	< 50	< 50	490	< 50	< 50	< 50	< 50	< 50
Br	0.5	< 0.5	< 0.5	< 0.5	< 0.5	< 0.5	< 0.5	< 0.5	< 0.5
Ca (%)	1.0	< 1	< 1	< 1	< 1	< 1	10.0	< 1	< 1
Co	1.0	11.0	12.0	8.0	14.0	21.0	17.0	13.0	15.0
Cr	5.0	31.0	46.0	38.0	8.0	47.0	64.0	32.0	53.0
Cs	1.0	< 1	< 1	< 1	< 1	< 1	< 1	< 1	< 1
Fe (%)	0.01	3.88	5.16	2.61	2.85	2.08	9.30	3.16	2.44
Hf	1.0	4.0	3.0	3.0	3.0	5.0	< 1	3.0	3.0
Hg	1.0	< 1	< 1	< 1	< 1	< 1	< 1	< 1	< 1
Ir	5.0	< 5	< 5	< 5	< 5	< 5	< 5	< 5	< 5
Mo	1.0	< 1	< 1	< 1	< 1	< 1	< 1	< 1	< 1
Na (%)	0.01	5.23	5.77	4.06	4.13	5.56	0.32	5.51	5.11
Ni	20.0	< 20	< 20	< 20	< 20	< 20	< 20	< 20	< 20
Rb	15.0	< 15	< 15	< 15	< 15	< 15	< 15	< 15	< 15
Sb	0.1	< 0.1	< 0.1	< 0.1	< 0.1	< 0.1	< 0.1	0.7	0.8
Sc	0.1	5.9	21.7	7.7	5.5	6.8	8.0	8.4	7.5
Se	3.0	< 3	< 3	< 3	< 3	< 3	< 3	< 3	< 3
Sn (%)	0.02	< 0.02	< 0.02	< 0.02	< 0.02	< 0.02	< 0.02	< 0.02	< 0.02
Sr (%)	0.05	< 0.05	< 0.05	< 0.05	< 0.05	< 0.05	< 0.05	< 0.05	< 0.05
Ta	0.5	< 0.5	< 0.5	< 0.5	< 0.5	< 0.5	< 0.5	< 0.5	< 0.5
Th	0.2	5.1	3.9	3.9	2.0	3.1	3.8	3.6	3.4
U	0.5	1.2	< 0.5	< 0.5	< 0.5	< 0.5	19.0	< 0.5	< 0.5
W	1.0	< 1	< 1	< 1	< 1	< 1	< 1	< 1	< 1
Zn	50.0	< 50	< 50	< 50	< 50	< 50	< 50	< 50	< 50
La	0.5	15.0	13.4	18.4	13.7	27.5	1230	36.2	21.6
Ce	3.0	21.0	22.0	24.0	18.0	34.0	1370.0	39.0	32.0
Nd	5.0	< 5	< 5	< 5	16.0	< 5	164	< 5	< 5
Sm	0.1	1.7	2.6	1.7	1.5	1.6	14.5	1.4	1.5
Eu	0.2	0.4	0.3	0.3	0.3	< 0.2	5.4	< 0.2	0.3
Tb	0.5	< 0.5	< 0.5	< 0.5	< 0.5	< 0.5	< 0.5	< 0.5	< 0.5
Yb	0.2	0.6	1.7	0.7	0.5	0.4	< 0.2	0.5	< 0.2
Lu	0.05	< 0.05	0.10	< 0.05	0.08	< 0.05	< 0.05	< 0.05	< 0.05

an adakitic composition and is distinct from normal island arc andesites, dacites, and rhyolites. The geochemical signature typical of the Newcastle Porphyry and other adakites results from shallow subduction of young, hot, buoyant oceanic slabs that are less than 25 million years old. In the case of Jamaica, rocks belonging to the CLIP underwent very shallow subduction beneath the Jamaican Arc (**Mitchell, 2020**), resulting in under-plating. At this point (80 Ma), the CLIP would have been only 10 million years old, having been erupted in the Pacific region at about 90 Ma (**Hastie et al., 2010**; **Abbott Jr. et al., 2013**). The trace element composition of the Newcastle Porphyry, and the geochemical models put forward by **Hastie et al. (2015)** suggest that the lavas are partial melts of a garnet amphibolite crust and there is no evidence that the lavas were generated by fractionation from a more mafic melt.

5.2 Geochemical Signature of the Newcastle Porphyry

The geochemistry of adakites reflects the characteristics of the source area. High SiO_2 (≥ 52 wt.%) and Al_2O_3 (≥ 7 wt.%) originate from the partial melting of the down-going CLIP whereas the low MgO (< 6 wt.%) indicates limited interaction of

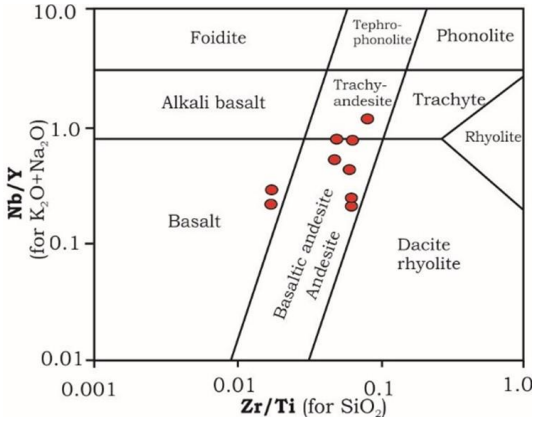

Figure 7. Nb/Y-Zr/Ti diagram (after Pearce, 2014) for the classification of volcanic rocks as proxy for the TAS diagram. Seven of nine samples plot within the basaltic andesite/ andesite and trachyandesite fields. The remaining two samples plot within the basalt field.

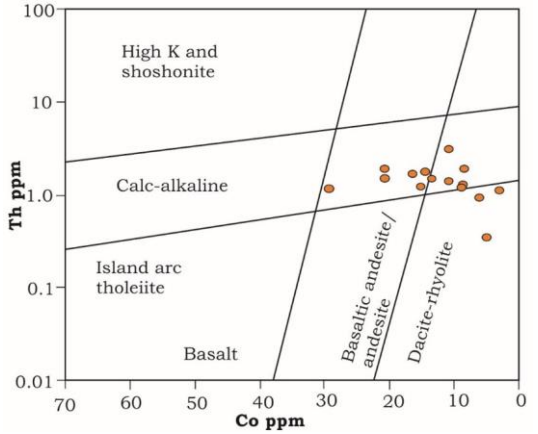

Figure 8. Th-Co diagram (after Hastie et al., 2007) for the classification of volcanic rock and volcanic series as proxy for K_2O-SiO_2 diagram. The Newcastle Porphyry plots preferentially as calc-alkaline basaltic andesites to dacites and rhyolites.

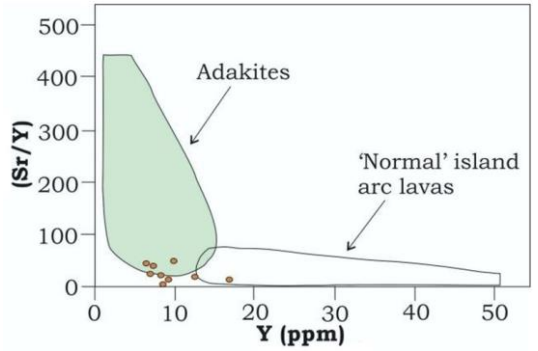

Figure 9. Sr/Y vs Y diagram used to discriminate adakites from normal island arc lava. Most of the Newcastle Porphyry samples analysed show low Sr/Y and plot within the adakite field. Modified from Martin (1999).

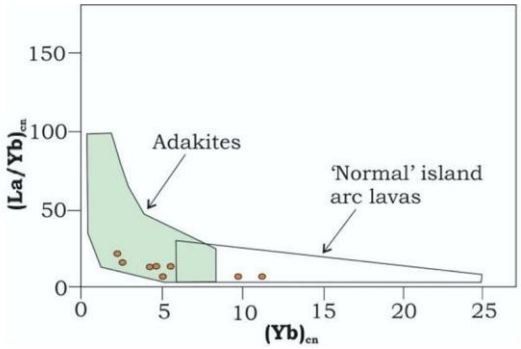

Figure 10. $(La/Yb)_{cn}$ vs Yb_{cn} diagram to discriminate adakites from normal arc lavas. Modified from Martin (1999).

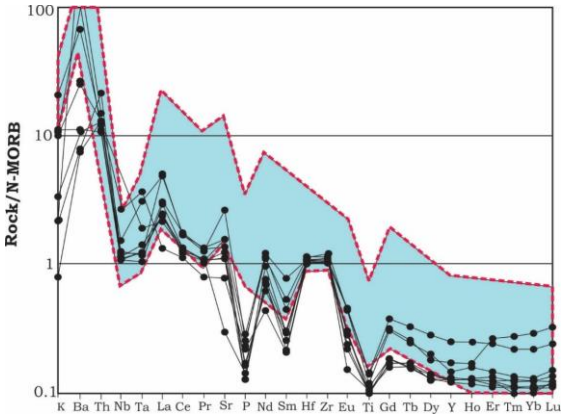

Figure 11. N-MORB-normalised multi-element spider diagram of the Newcastle Porphyry. Normalising values from McDonough and Sun (1995). The outlined field represents Archean and Cenozic adakites data from Defant et al. (1991, 1992). The trace element pattern for the Newcastle Porphyry, with only a few exceptions, corresponds closely with that of Archean adakites (TTG/D) and Cenozoic adakites.

the resultant melt with any potential peridotite mantle wedge. The trace element characteristics of adakites are defined by low Y and HREE, high Sr that rarely trends below 400 ppm, low HFSE, high Cr (~ 36 ppm), and high Ni (~ 24 ppm) (Defant and Drummond, 1990); the Sr/Y ratio in adakites as defined by **Defant and Drummond (1990)** is 40. The Sr/Y ratio in adakites can be explained by slab melting under high pressure and the subsequent release of Sr from plagioclase into the melt. On the other hand, residual garnet can hold on to Y during partial melting at higher pressure. This results in high concentrations of Sr in the melt relative to Y (**Martin and Moyen, 2002**; **Moyen, 2009**).

The Newcastle Porphyry shows some deviation from the typical adakites described above and has been termed Jamaican-type adakite or JTA by **Hastie et al. (2010)**. When compared to adakites worldwide, the Newcastle Porphyry has lower Sr

Table 4. Comparison of the geochemistry of average Fe skarn plutons with data from three selected deposits

Parameter	Calcic Fe Skarn Pluton, worldwide averages, (Meinert, 1995)	Newcastle Porphyry (this study)	Fe skarn pluton, British Columbia (Ray et al., 1995)	Fe skarn Pluton, Hierro Indio, Argentina (Pons et al., 2010)
MgO wt.%	3.0	1.66	2.9	2.18
K_2O wt.%	2.10	0.88	1.45	1.20
Al_2O_3 wt.%	16.8	16.5	16.3	18.0
Fe_2O_3 wt.%	2.8	5.95	7.87	2.9
Ni ppm	35	19	-	13
V ppm	152	74	163	80
Sc ppm	17	8	27	10
Rb/Sr	0.08	0.07	0.04	0.04

(59-463 ppm) and correspondingly low Sr/Y ratios of 7-48. The lack of a positive Sr anomaly in the Newcastle Porphyry can be attributed to the presence of residual plagioclase in the source area that acts as a buffer to Sr in the melt (**Hastie et al., 2010**; **Sun et al., 2015**). The Ni content of the Newcastle Porphyry ranges from 10.5 to 37.2 ppm with a mean of 19 ppm. Nickle substitutes almost exclusively into olivine (**Meinert, 1995**; **Pons et al., 2010**). The relatively low concentration of Ni in the Newcastle Porphyry compared to other adakites suggests that the source region had a low Ni content. Hornblende and feldspar are main K-bearing minerals (**Sun et al., 2015**). Though k-feldspar and hornblende are two of the main phenocrysts in the Newcastle Porphyry, low K_2O is likely due to the low K content of the source material, the CLIP. The Newcastle Porphyry has a characteristically low concentration of HREEs. HREEs tend to be fractionated into amphibole during crystallisation or held in residual garnet (**Pons et al., 2010**; **Rollins, 1993**). These geochemical characteristics, along with low MgO and Cr make the Jamaican-type adakites very similar to early Archean tonalites-trondhjemites-granodiorites/dacites (TTG/D) which are the ancient equivalents of modern adakites (**Martin and Moyen, 2002**; **Hastie et al., 2010**; **Castillo, 2012**). Nevertheless, the chondrite normalised values of trace elements show that the Newcastle Porphyry has anomalously low concentrations of Ti, LREE, Nb, Ta, P, and Ba relative to Archean and Cenozoic adakites.

5.3 Comparison of Newcastle Porphyry with average Fe Skarn Plutons

Several authors have conducted research on the geochemistry of plutons associated with skarn deposits including **Meinert** (**1995**), **Meinert** (**1984**), **Pons et al.** (**2010**), and **Ray et al.** (**1995**) in an effort to identify a relationship between skarn type and the petrogenesis of the causative pluton. In his study, **Meinert** (**1995**), analysed 157 samples of igneous rocks associated with skarns worldwide and identified geochemical characteristics typical of each type of skarn. Plutons associated with calcic Fe skarns such as those at Mavis Bank tend to be normal calc-alkaline with higher MgO and K_2O, suggesting a primitive magma source. These plutons also tend to be the least Al saturated when compared to other skarns and tend to cluster around the boundary between metaluminous and peraluminous; they are, however, rarely peralkaline. In fact, **Meinert** (**1995**) described plutons associated with calcic Fe skarns as having a strong mantle signature and showing little contamination from sedimentary rocks. Similarly, **Pons et al.** (**2010**) and **Ray et al.** (**1995**), from their studies on Fe skarns in the Andes and British Columbia respectively, both concluded that Fe skarns are associated with mafic to intermediate plutons of calc-alkaline setting with geochemistry suggesting primitive magmas. **Meinert** (**1995**) described the lack of a crustal signature in Fe skarn plutons as reminiscent of tholeiitic MORB. The trace element characteristics of these plutons include high compatible elements such as Ni, V, and Sc and Rb/Sr ratios that are generally less than 1. **Table 4** shows a comparison of selected major- and trace elements data for the Newcastle Porphyry, with Fe skarn plutons in Argentina and British Columbia as well for mean Fe skarn plutons worldwide. The data show that the concentrations of MgO and K_2O in the Newcastle Porphyry are considerably less than for typical calcic Fe skarns. A plot of these major elements versus SiO_2 (**Figures 12-13**) further illustrates this. The major element data in these plots show data from this study as well as results obtained from **Hastie et al.** (**2010**). Data for average Cu skarn plutons are also added for comparison. The graphs show that the major element concentration of the Newcastle Porphyry does not correlate well with those of typical Fe skarn plutons. Instead, they show a very strong crustal signature with major element concentrations reflecting the adakite genesis.

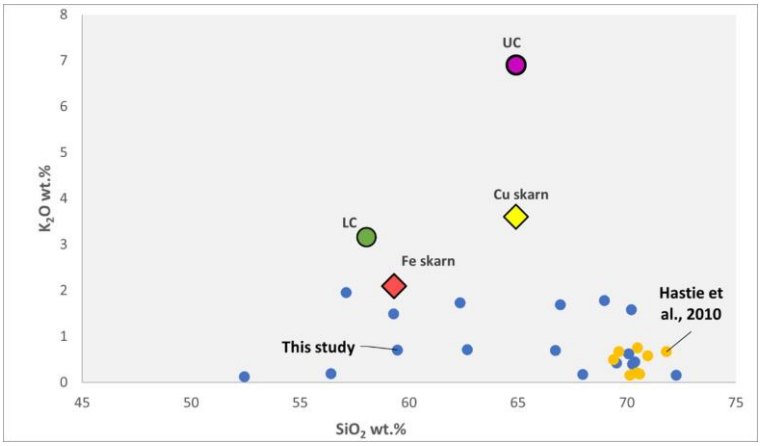

Figure 12. SiO_2 vs K_2O diagram showing the average geochemistry of Fe skarn plutons (Meinert, 1995), compared with geochemistry of Newcastle Porphyry after this study (blue), after Hastie et al. (2010) and the upper crust (UC) and lower crust (LC) averages (Wedepohl, 1995).

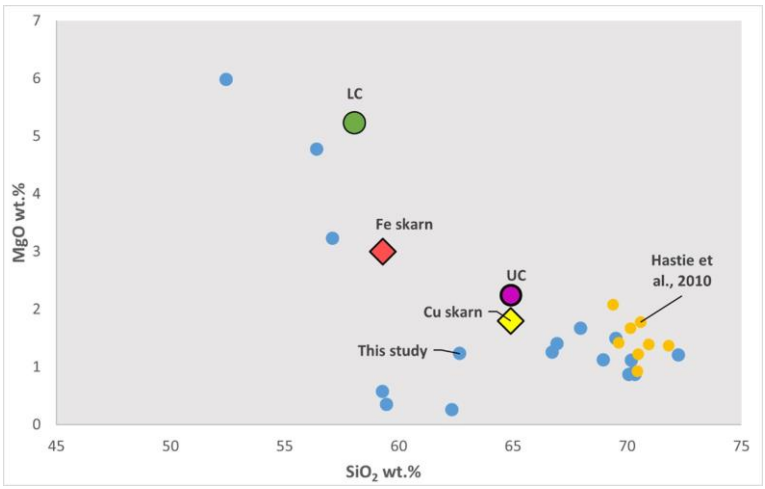

Figure 13. SiO_2 vs MgO diagram showing the average geochemistry of Fe skarn pluton (Meinert, 1995), compared with geochemistry of Newcastle Porphyry after this study (blue), after Hastie et al. (2010) and the upper crust (UC) and lower crust (LC) averages (Wedepohl, 1995).

It has been shown that there is a relationship between skarn types and the degree of differentiation of the associated plutons. Plutons associated with Fe (as in the case of the Newcastle Porphyry) and Au skarns are the least differentiated and are most similar to primitive melts. At the other end of the spectrum, Mo and W skarns are associated with highly fractionated plutons (**Meinert, 1995**). **Figure 14** shows the range of trace element concentrations associated with typical Fe skarn plutons. The range for Cu skarn plutons, which are moderately differentiated, is shown for comparison. Rubidium and Sc behave differently during the differentiation process; the concentration of Sc is highest during the early stages of crystallisation since it substitutes into clinopyroxene as crystallisation proceeds. As differentiation proceeds, Rb content increases in the melt because it is incompatible. Primitive plutons typical of Fe skarns will therefore have relatively high Sc and low Rb compared to highly differentiated plutons. Vanadium substitutes into magnetite and ilmenite and Ni substitutes into olivine, and these will therefore be present at relatively high concentrations in more primitive plutons. High Rb/Sr is typical of plutons associated with Sn, Mo, and W skarns whereas low Rb/Sr ratios are typical of Fe skarns. Like Rb, Ba will substitute into K-feldspars and micas and will be present at higher concentrations in plutons that are more differentiated and will be depleted in more primitive melts (**Meinert, 1995**; **Pons et al., 2010**). The plots of these trace elements indicate that the Newcastle Porphyry, though not a primitive rock, has trace element signatures very similar to other plutons associated with Fe skarns.

5.4 Mineral Deposit Associations of Adakitic Rocks

Adakites have been known to produce world class skarns, including calcic Fe skarns. For example, in the Handan-Xingtai district of the North China Craton, Fe-Cu skarn mineralisation is genetically related to granitic to dioritic plutons with major and trace element signatures similar to adakites (**Sun et al., 2015**). These polymetallic deposits are important world class skarn deposits that have been

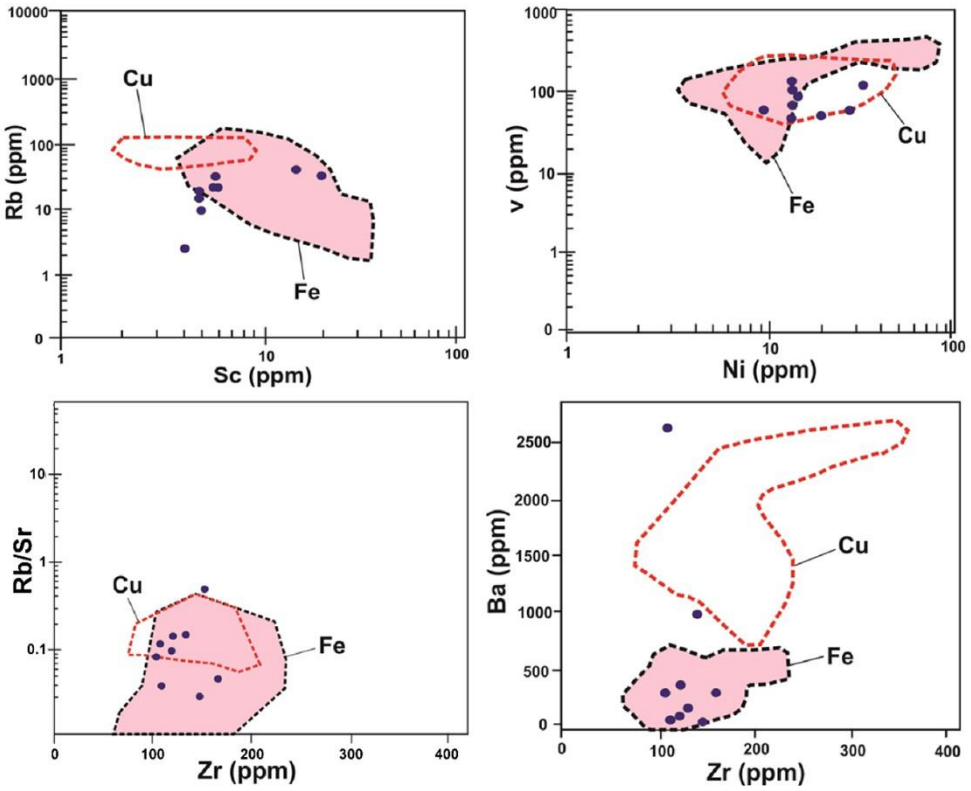

Figure 14. Trace element plot for the Newcastle Porphyry. Ranges for plutons associated with Fe skarn plutons and Cu skarn plutons (after Meinert, 1995) are outlined for comparison. A: Rb vs Sc. B: V vs Ni. C: Rb/Sr vs Zr. D: Ba vs Zr. The trace element composition of the Newcastle Porphyry falls within the general range expected for Fe skarn plutons.

reported to have over 700 Mt iron (**Deng et al., 2015**). Similarly, adakitic plutons have been observed associated with Au-Fe skarns in the Mezcala deposit in Mexico and with Cu-Mo skarns from Mivehrood, Iran. These adakitic plutons, like the Newcastle adakites are calc-alkaline intermediate to felsic igneous rocks (**Gonzalez-Partida et al., 2003**; **Alirezaei et al., 2016**).

Meinert (**1984**) noted that there is a difference between plutons related to calcic Fe skarns and plutons related to other skarns. The author also showed via illustration that the Fe content of typical skarn plutons in British Columbia was generally lower than normal igneous rocks. From this, it can be concluded that the comparatively lower Fe content of adakitic plutons does not preclude it from forming Fe skarns. In fact, **Meinert** (**1984**) concluded that the amount of Fe in hydrothermal fluids and the resultant concentration of Fe in skarns is strongly correlated to the chlorine content, oxidation state, and temperature of the hydrothermal solution and less dependent on the total Fe content of the pluton. Adakites have been known to have a close relationship with porphyry Au-Cu deposits world-wide and are considered to be more metalliferous than other magmas by virtue of the magmas being more oxidised, with a higher S and water content (**Sojona and Maury, 1998**; **Mungall, 2002**; **Zhang et al., 2019**). Controversy however exists as to whether these deposits are the result of slab melts or whether the magmatic-hydrothermal process has imparted adakite like signatures on normal arc rocks in these ore zones (**Castillo, 2012**). Nevertheless, the high silica content and viscosity of adakites cause them to be more susceptible to crustal entrapment and subsequent development of effective hydrothermal systems than normal ADRs (**Sojona and Maury, 1998**).

6. Conclusion

Outcrops of the Newcastle Porphyry in the Mavis Bank area of St Andrew have been shown to be spatially and genetically related to calcic Fe skarns which occur as massive and disseminated magnetite with minor Cu and Co in limestones and shales. The mineralogy of the Newcastle Porphyry is dominated by plagioclase, hornblende, and quartz and in some areas, has been affected by extensive propylitic and

sericitic alteration.

The petrogenesis of the Newcastle Porphyry has been deduced using trace and major element geochemistry. The trace element data point to extensive calc-alkaline volcanism in the Wag Water trough with rock compositions ranging from andesite to dacite-rhyolite. These igneous rocks have also been shown to have an adakitic composition which distinguishes them from regular ADRs. Among other characteristics, "Newcastle adakites" have negative Ta and Nb anomalies and low HREE concentrations which occur as a result of high pressure residual phases. The major element composition of the Newcastle Porphyry does not fit to a great extent the geochemical characteristics typical of calcic Fe skarn plutons worldwide. Instead, the major element composition is more reflective of a high crustal signature typical of adakites, but atypical of Fe skarn plutons. On the other hand, the concentration of trace elements such as Ba, Sr, Rb, Sc, Ni, and V are within the ranges typical of Fe skarn plutons that have geochemical signatures akin to primitive magmas. Although adakitic plutons differ in some respects from typical Fe skarn plutons, they are associated with world-class skarn deposits in China and North America. Overall, adakites are considered very metalliferous and are commonly associated with porphyry and other polymetallic deposits.

Acknowledgements. The authors are grateful for the assistance given by Norris Whyte and Shane Wedderburn in the field. We thank the reviewers who were thorough and thoughtful in helping to improve this manuscript. We also thank the Editor for accepting this manuscript for publication.

Funding. This paper is based on research conducted in fulfilment of the requirements of a Master of Philosophy Degree in Geology from the University of the West Indies (UWI), Mona. The authors thank the School of Graduate Studies at UWI Mona for providing general funding for this research, the University of New Brunswick for providing analyses using micro-XRF and LAICPMS analyses, and the Mines and Geology Division Laboratory for providing sample preparation and major element analysis.

Authors Contributions. TB – Main author of manuscript. Conducted literature review and data interpretation. Create maps, figures, and tables. SM – Thesis Supervisor. Reviewed and edited manuscript. Gave technical guidance and advice to main author. Contributed to the geology section of manuscript. Edited figures and maps. DL – Reviewed and edited manuscript. Gave technical guidance to main author. Assisted in sourcing various literature. Funded trace element analysis (INAA), polished thin sections and partial funding of LAICPMS analysis.

Data availability statement. All analytical results are included in this paper.

REFERENCES

Abbott Jr, R.N., Bandy, B.R. and Rajkumar, A. 2013. Cenozoic burial metamorphism in eastern Jamaica. *Caribbean Journal of Earth Science*, **46**, 13-30.

Alirezaei, S., Einali, M., Jones, P., Hassanpour, S. and Arjmandzadeh, R. 2016. Mineralogy, geochemistry, and evolution of the Mivehrood skarn and the associated pluton, northwest Iran. *International Journal of Earth Science*. **105**, 849-868. https://doi.org/10.1007/s00531-015-1200-4

Blaise, J. and Fenton, A. 1976. *Preliminary investigation of Mavis Bank copper prospect. Economic Geology Report* No. 5. 56 pp. Mines and Geology Division, Kingston.

Castillo, P.R. 2006. An overview of adakite petrogenesis. *Chinese Science Bulletin*, **51**, 257-268. https://doi.org/10.1007/s11434-006-0257-7

Castillo, P.R. 2012. Adakite petrogenesis. *Lithos*, **34**, 304-316. https://doi:10.1016/j.lithos.2011.09.013

Defant, M.J. and Drummond, M.S. 1990. Derivation of some modern arc magmas by melting of young subducted lithosphere. *Nature*, **347**, 662-665. https://doi.org/10.1038/347662a0

Deng, X.-D., Li, J.-W. and Wen, G. 2015. U-Pb geochronology of hydrothermal zircons from the Early Cretaceous iron skarn deposits in the Handan-Xingtai District, North China Craton. *Economic Geology*, **110**, 2159-2180. https://doi.org/10.2113/econgeo.110.8.2159

Gonzalez-Partida, E., Levresse, G., Carrillo-Chávez, A., Cheilletz, A., Gasquet, D. and Solorio-Munguía, J. 2003. (Au-Fe) Skarn deposits of the Mezcala District, south-central Mexico: adakite association of the mineralising fluids. *International Geological Review*, **45**, 79-93. https://doi.org/10.2747/0020-6814.45.1.79.

Hall, G.E.M. 1992. Inductively coupled plasma mass spectrometry in geoanalysis. *Journal of Geochemical Exploration*, **44**, 201-249. https://doi.org/10.1016/0375-6742(92)90051-9

Hastie, A.R., Kerr, A.C., Pearce, J.A. and Mitchell, S.F. 2007. Classification of altered volcanic island arc rocks using immobile trace elements: development of the Th–Co discrimination diagram. *Journal of Petrology*, **48**, 2341-2357.

Hastie, A.R. and Kerr, A.C. 2010. Mantle plume or slab window?: Physical and geochemical constraints on the origin of the Caribbean Oceanic Plateau. *Earth Science Review*, **98**, 283-293. https://doi.org/10.1016/j.earscirev.2009.11.001.

Hastie, A.R., Kerr, A.C., McDonald, I., Mitchell, S.F., Pearce, J.A., Millar, I.L., Barfod, D. and Mark, D.F. 2010. Geochronology, geochemistry and petrogenesis of rhyodacite lavas in eastern Jamaica: a new adakite subgroup analogous to Early Archaean continental crust? *Chemical Geology*, **276**, 344-359. https://doi.org/10.1016/j.chemgeo.2010.07.002.

Hastie, A.R., Mitchell S.F., Kerr, A.C., Minifie, M.J. and Millar, I.L. 2011. Geochemistry of rare high-Nb basalt lavas: are they derived from a mantle wedge metasomatised by slab melts? *Geochemica et Cosmochemica Acta*, **75**, 5049-5072. https://doi.org/10.1016/j.gca.2011.06.018

Hastie, A.R., Fitton, J.G., Mitchell, S.F., Neill, I., Nowell, G.M. and Millar, I.L. 2015. Can fractional crystallisation, mixing and assimilation processes be responsible for Jamaican-type adakites? implications for generating Eoarchaean continental crust. *Journal of Petrology*, **56**, 1251-1284. https://doi.org/10.1093/petrology/egv029

Hoffman, E.L. 1992. Instrumental neutron activation in geoanalysis. *Journal of Geochemical Exploration*, **44**, 297-319. https://doi.org/10.1016/0375-6742(92)90053-B

Jackson, T.A. 1987. The petrology of Jamaican Cretaceous and Tertiary volcanic rocks and their tectonic significance. In **R. Ahmad (Ed.)**, *Proceedings of a Workshop on the Status of Jamaican Geology*. Kingston. Geological Society of Jamaica, Special Issue, 107-119

Jackson, T.A. and Smith, T.E. 1978. Metasomatism in the Tertiary volcanics of the Wagwater Belt, Jamaica. *Geologie en Mijnbow*, **57**, 213-220.

James-Williamson, S.A., Mitchell, S.F. and Ramsook, R. 2014. Tectono-stratigraphic development of the Coastal Group of south-eastern Jamaica. *Journal of South American Earth Sciences*, **50**, 40-47.

Jenner, G.A. 1996. Trace element geochemistry of igneous rocks: geochemical nomenclature and analytical geochemistry. In **D.A. Wyman (Ed)**, *Trace Element Geochemistry of Volcanic Rocks: applications for massive sulfide exploration, GAC Short Course* **12**, 51-77.

Kerr, A.C., Iturralde-Vinent, M.A., Saunders, A.D., Babbs, T.L. and Tarney, J. 1999. A new plate tectonic model of the Caribbean: implications from a geochemical reconnaissance of Cuban Mesozoic volcanic rocks. *Geological Society of America Bulletin*, **111**, 1581-1599. https://doi.org/10.1130/0016-7606(1999)111<1581:ANPTMO>2.3.CO;2

Laznicka, P. 2006. *Giant Metallic Deposits: Future Sources of Industrial Metals*. 731 pp. New York: Springer.

Mann, P. and Burke, K. 1990. Transverse intra-arc rifting: Palaeogene Wagwater Belt, Jamaica. *Marine and Petroleum Geology*, **7**, 410-427. https://doi.org/10.1016/0264-8172(90)90018-c

Martin, H. 1999. Adakitic magmas: modern analogues of Archaean granitoids. *Lithos*, **46**, 411-429. https://doi.org/10.1016/S0024-4937(98)00076-0

Martin, H. and Moyen, J.-F. 2002. Secular changes in tonalite–trondhjemite–granodiorite composition as markers of the progressive cooling of Earth. *Geology*, **30**, 319–322. https://doi.org/10.1130/0091-7613(2002)030<0319:SCITTG>2.0.CO;2

Matley, C. A. 1940. The geology of the Kingston district, Jamaica. *Abstracts of the Proceedings of the Geological Society of London*, **1373**, 99-106.

McDonough, W.F. and Sun S.-S. 1995. The composition of the earth. *Chemical Geology*, **120**, 223-253. https://doi.org/10.1016/0009-2541(94)00140-4

Meinert, L.D. 1984. Mineralogy and petrology of iron skarns in western British Columbia, Canada. *Economic Geology*, **79**, 869-882. https://doi.org/10.2113/gsecongeo.79.5.869

Meinert, L.D. 1992. Skarns and skarn deposits. *Geoscience Canada*, **19**, 145-162. https://doi.org/10.2113/gsecongeo.79.5.869

Meinert, L.D. 1995. Compositional variation of igneous rocks associated with skarn deposits-chemical evidence for a genetic connection between petrogenesis and mineralisation. *Mineralogical Association of Canada Short Course Series*, **23**, 401-418.

Meinert, L.D. 1997. Application of skarn deposit zonation models to mineral exploration. *Exploration and Mining Geology*, **6**, 185-208.

Meinert, L.D., Dipple, G.M. and Nicolescu, S. 2005. World skarn deposits. *Economic Geology 100th Aniversary Volume*, 299-336. https://doi.org/10.5382/AV100.11

Mitchell, S. F. 2003a. Sedimentology and Tectonic Evolution of the Cretaceous Rocks of Central Jamaica: Relationships to the Plate Tectonic Evolution of the Caribbean. In: **C. Bartolini, R. T. Buffler and J. F. Blickwede (Eds.)**, *The Circum-Gulf of Mexico and the Caribbean: hydrocarbon habitats, basin formation, and plate tectonics. American Association of Petroleum Geologists Memoir*, **79**, 605-623, Tulsa, Arizona, USA.

Mitchell, S.F. 2003b. Lithostratigraphy and palaeogeography of the White Limestone Group. *Cainozoic Research*, **3** (1/2), 5-29.

Mitchell, S. F. 2006. Timing and implications of Late Cretaceous tectonic and sedimentary events in Jamaica. *Geologica Acta*, **4**, 171-178.

Mitchell, S.F. 2020. Cretaceous geology and tectonic assembly of Jamaica. *Geological Society, London, Special Publications*, **504**. https://doi.org/10.1144/SP504-2019-210

Mitchell, S.F. 2021. The first Paleogene transgression onto the Clarendon Block (Jamaica). *Caribbean Journal of Earth Science*, **53**, 1-10.

Moyen, J.F. 2009. High Sr/Y and La/Yb ratios: the meaning of the "adakitic signature". *Lithos*, **112**, 556-574. https://doi.org/10.1016/j.lithos.2009.04.001

Mungall, J.E. 2002. Roasting the mantle: Slab melting and the genesis of major Au and Au-rich Cu deposits. *Geology*, **30**, 915-918. https://doi.org/10.1130/0091-7613(2002)030<0915:RTMSMA>2.0.CO;2

Murphy, M.A. and Salvador, A. 1998. International Stratigraphic Guide — An abridged version. *Episodes*, **22**, 255-271.

Pearce, J.A. 2014. Immobile element fingerprinting of ophiolites. *Elements*, **10**, 101-108. https://doi.org/10.2113/gselements.10.2.101

Pindell, J.L. 1994. Evolution of the Gulf of Mexico and the Caribbean. In: **S.K. Donavon and T. Jackson (Eds.)**, *Caribbean Geology: An Introduction*, p. 13-39, UWI Publishers' Association, Kingston, Jamaica.

Pindell, J.L., Kennan, L., Stanek, K.P., Maresch W.V. and Draper, G. 2006. Foundations of Gulf of Mexico and Caribbean evolution: eight controversies resolved. *Geologica Acta*, **4**, 303-341. https://doi.org/10.1344/105.000000371

Pindell, J. and Kennan, L. 2009. Tectonic evolution of the Gulf of Mexico, Caribbean and northern South America in the mantle reference frame: an update. In:

K.H. James, M.A. Lorente, and J.L. Pindell (Ed.), ,*Geological Society London, Special Publications*, **328**, 1–55. https://doi.org/10.1144/SP328.1

Pirajno, F. 2009. *Hydrothermal processes and mineral systems*. 580 pp. Springer, Perth.

Pons, J., Franchini, M., Meinert, L., López-Escobar, L. and Maydagán, L. 2010. Geology, petrography and geochemistry of igneous rocks related to mineralised skarns in the NW Neuquén Basin, Argentina: implications for Cordilleran skarn exploration. *Ore Geology Review*, **38**, 37-58. https://doi.org/10.1016/j.oregeorev.2010.05.006

Ray, G.E., Webster, I.C.L. and Ettlinger, A.D. 1995. The distribution of skarns in British Columbia and the chemistry and ages of their related plutonic rocks. *Economic Geology*, **90**, 920-937. https://doi.org/10.2113/gsecongeo.90.4.920

Robinson, E. 1994. Jamaica. In: **S.K. Donavon and T. Jackson (Eds.)**, *Caribbean Geology: an introduction*, p. 111-128, UWI Publishers' Association, Kingston, Jamaica.

Robinson, E. and Mitchell, S.F. 1999. Middle Eocene to Oligocene Stratigraphy and Palaeogeography in Jamaica: A Window on the Nicaragua Rise. Fourth Annual Meeting of IGCP 393, 12-18 July, 1999. *Contributions to Geology, UWI, Mona*, **#4**, 1-47.

Robinson, E., Lewis, J.F. and Cant, R.V. 1970. Field guide to aspects of the geology of Jamaica. *International Field Institute Guidebook to the Caribbean Island Arc System*, 1-48.

Rollinson, H. 1993. *Using Geochemical Data: Evaluation, Presentation, Interpretation*. 384 pp. London: Longman Scientific & Technical.

Roobol, M.J. 1971. The volcanic geology of Jamaica. *Transactions of the 6th Caribbean Geological Conference, Margarita, Venezuela*, 100-107.

Roobol, M.J. 1975. Caribbean keratophyre. *3rd Latin American Geology Conference*. 3630-3641.

Sajona, F.G. and Maury, R.C. 1998. Association of adakites with gold and copper mineralisation in the Philippines. *Comptes Rendus de l'Académie des Sciences*, **326**, 27–34. https://doi.org/10.1016/S1251-8050(97)83200-4

Sun, Y., Xiao L., Zhan, Q., Wu, J., Zhu, D., Huang, W., Bai, M. and Zhang, Y. 2015. Petrogenesis of the Kuangshancun and Hongshan intrusive complexes from the Handan–Xingtai District: implications for iron mineralisation associated with Mesozoic magmatism in the North China Craton. *Journal of Asian Earth Science*, **113**, 1162-1178. https://doi.org/10.1016/j.jseaes.2015.08.003

Vincenz, S.A. 1955. Magnetic prospecting for iron ores in Jamaica. *Geophysics*, **20**, 593-614.

Wedepohl, K.H. 1995. The composition of the continental crust. *Geochemica et Cosmochemica Acta*, **59**, 1217-1232. https://doi.org/10.1016/0016-7037(95)00038-2

Zans, V.A. 1955. Preliminary report on iron-ore deposits at Glade-Orchard near Mavis Bank, St. Andrew. Appendix A. In: *Annual Report 1953-1954*, p. 15-19. Geological Survey Department, Jamaica.

Zhang, L., Li, S. and Zhao, Q. 2019. A review of research on adakites. *International Geology Review*, 63, 47-64. https://doi.org/10.1080/00206814.2019.1702592

Editorial Responsiblity: Dr S. James-Williamson. Type setting: Prof. S. F. Mitchell

Accepted 26th April 2022